ЖЭТФ, 2013, том 144, вып. 5 (11), стр. 921–930 

# SPATIAL STRUCTURE OF A COLLISIONALLY INHOMOGENEOUS BOSE–EINSTEIN CONDENSATE

*Fei Li*[a,b*], *Dongxia Zhang*[c], *Shiguang Rong*[c], *Ying Xu*[c]

[a] *Department of Education Science, Hunan First Normal University 410205, Changsha, China*

[b] *Key Laboratory of Low-Dimensional Quantum Structures and Quantum Control, Ministry of Education, Hunan Normal University 410081, Changsha, China*

[c] *Department of Physics, Hunan University of Science and Technology 411201, Xiangtan, China*

Received April 28, 2013

The spatial structure of a collisionally inhomogeneous Bose–Einstein condensate (BEC) in an optical lattice is studied. A spatially dependent current with an explicit analytic expression is found in the case with a spatially dependent BEC phase. The oscillating amplitude of the current can be adjusted by a Feshbach resonance, and the intensity of the current depends heavily on the initial and boundary conditions. Increasing the oscillating amplitude of the current can force the system to pass from a single-periodic spatial structure into a very complex state. But in the case with a constant phase, the spatially dependent current disappears and the Melnikov chaotic criterion is obtained via a perturbative analysis in the presence of a weak optical lattice potential. Numerical simulations show that a strong optical lattice potential can lead BEC atoms to a state with a chaotic spatial distribution via a quasiperiodic route.

**DOI**: 10.7868/S0044451013110047

## 1. INTRODUCTION

Ever since Dahan et al. successfully loaded Bose–Einstein condensates (BECs) in optical lattices [1, 2], the rich and interesting phenomena of BECs in optical lattices attract more and more attention. This is because BECs in optical lattices open up numerous new research aspects for both fundamental and applied problems in quantum mechanics. An optical lattice can be created by the interference of two or more laser beams [3]. Many important phenomena following from the interactions between BECs and optical lattices have been profoundly investigated, both experimentally and theoretically. A quantum phase transition in a BEC with repulsive interactions, confined in a three-dimensional optical lattice potential, was found in [4]. As the potential depth increases, a transition is observed from a current to a Mott-insulator phase [4]. In one-dimensional ($1D$) off-resonance optical lattices, for small values of the lattice well depth, Bloch oscillations were observed [5]. Using the Holstein–Primakoff (HP) transformation, Xie and coworkers theoretically found that the dark and bright magnetic solitons can exist in spinor BECs in a $1D$ optical lattices in different parameter regions [6]. Up to date, the intriguing BEC phenomena investigated experimentally or theoretically in optical lattices include current and dissipative dynamics [7], arrays of Josephson junctions [8], Landau–Zener tunneling [2, 9–12], squeezed states [13], chaos [14–30], and so on. In recent years, BECs in traveling optical lattices also receive considerable attention [29–39].

It is undoubted that the spatial structure of BECs — the spatial distribution of condensed atoms — is of great importance to various phenomena exhibited by BECs. The spatial chaos of a trapped BEC in a $1D$ weak optical lattice was studied in [19], followed by the research on spatial chaos of BECs in a Wannier–Stark potential [20]. In our previous works, the spatial chaos of BECs in a cigar-shaped trap and an asymmetric periodic potential were investigated [21]. The

*E-mail: wiself@gmail.com

spatial chaos discussed in the above papers can be attributed to the same type, continuous spatial chaos. Recently, a different type of spatial chaos defined as a discrete chaotic state was announced [18]. The authors presented analytic evidence of this type of spatial chaos in a $1D$ attractive BEC [18]. In the study of the two types of spatial chaos, both the amplitudes and signs of the nonlinearity parameters in the above references are space-independent [18–21]. However, experiments have demonstrated that the nonlinearity parameter can be adjusted from large negative values to large positive values via a technique named the Feshbach resonance [40–45]. In early years, the time-dependent nonlinearity parameters were usually considered [25, 40–44].

Recently, the realization and the role of a spatially varying nonlinearity were discussed in [46–48] and the references therein. BECs with spatially varying nonlinearities are usually called collisionally inhomogeneous ones [45, 49, 50]. To the best of our knowledge, the role of spatially varying nonlinearities in the spatial distribution of condensed atoms has not been reported so far. In this paper, we address this problem. As is known, many properties of BECs, including the spatial distribution of condensed atoms, are badly influenced by the nonlinearity parameter. Therefore, studies on the role of the spatially varying nonlinearities in the spatial distribution of BEC atoms are necessary.

This paper is organized as follows. In Sec. 2, the case with a spatially dependent phase is considered. We find that there exists a spatially varying current with an explicit analytic expression in the system, and a strong oscillation of the current induces a very complex spatial structure in the systems. In Sec. 3, the case with a constant phase is considered. A perturbative analysis is performed and the Melnikov chaotic criterion is obtained. Numerical simulations demonstrate that the system steps from a quasiperiodic state into a chaotic one as the depth of the external optical lattice potential increases. In Sec. 4, a brief conclusion is presented.

## 2. THE CASE WITH A SPATIALLY DEPENDENT PHASE

In the mean-field approximation, the dynamics of a quasi-$1D$ BEC can be modeled by a $1D$ Gross–Pitaevskii equation

$$i\hbar\frac{\partial\psi}{\partial t} = -\frac{\hbar^2}{2m}\frac{\partial^2\psi}{\partial x^2} + V_{ext}(x)\psi + g|\psi|^2\psi, \qquad (1)$$

where $m$ is the atom mass, $\hbar$ is the Planck constant, $V_{ext}(x)$ is the external potential, $\psi$ is the macroscopic quantum wave function characterizing the dynamical evolution of BEC near zero temperature,

$$g = 2\hbar\omega_\perp a_s$$

is the nonlinearity parameter characterizing the two-particle interaction, and $a_s$ is the $s$-wave scattering length: $a_s > 0$ indicates a repulsive interaction and $a_s < 0$ corresponds to an attractive interaction.

In this paper, we consider the sine optical lattice potential

$$V_{ext}(x) = V_1 \sin(2Kx), \qquad (2)$$

where $K$ is the wave vector of the lasers forming the optical potential. Such an optical potential can be created by the interference of two or more laser beams.

For simplicity, we adopt the dimensionless variables

$$\begin{aligned} &\tilde{t} = \frac{\hbar}{m}[K]^2 t, \quad \tilde{x} = [K]x, \quad \tilde{\psi} = \frac{\psi}{\sqrt{n}}, \\ &\tilde{V}_1 = \frac{m}{[K]^2\hbar^2}V_1, \quad \tilde{K} = \frac{K}{[K]}, \quad \tilde{g} = \frac{mn}{[K]^2\hbar^2}g, \end{aligned} \qquad (3)$$

where $n$ is the density of atoms in the BEC and $[K]$ is the unit of $K$. It is convenient, and hopefully does not result in misunderstanding, to replace $\tilde{t}$ with $t$, etc. Then the Gross–Pitaevskii equation in dimensionless form becomes

$$i\frac{\partial\psi}{\partial t} = -\frac{1}{2}\frac{\partial^2\psi}{\partial x^2} + V_1\sin(2Kx)\psi + g|\psi|^2\psi. \qquad (4)$$

It has been pointed out that the spatial modulation of the scattering length can be achieved via the Feshbach resonance technique, which means that the nonlinearity parameter $g$ can be spatially dependent [46–48]. In this paper, we consider the nonlinearity parameter of the form

$$g(x) = g_0 + g_1\sin^2(\kappa x), \qquad (5)$$

where $g_0$ is the value of the nonlinearity parameter in the absence of modulation, and $g_1$ and $\kappa$ are the amplitude and wavenumber of the modulation.

Performing the transformation

$$\phi = \sqrt{g(x)}\psi \quad \text{for} \quad g(x) \neq 0,$$

we arrive at [45, 46]

$$i\frac{\partial\phi}{\partial t} = -\frac{1}{2}\frac{\partial^2\phi}{\partial x^2} + |\phi|^2\phi + V_1\sin(2Kx)\phi + \hat{V}_{eff}(x)\phi, \qquad (6)$$

$$\hat{V}_{eff}(x) = \frac{1}{2\sqrt{g}}\frac{\partial^2\sqrt{g}}{\partial x^2} - \frac{1}{g}\left(\frac{\partial\sqrt{g}}{\partial x}\right)^2 + \\ + \frac{1}{\sqrt{g}}\frac{\partial\sqrt{g}}{\partial x}\frac{\partial}{\partial x}. \quad (7)$$

For the weak modulation with $g_0 \gg g_1$, $\hat{V}_{eff}(x)$ can be expressed as

$$\hat{V}_{eff}(x) = -\frac{3\kappa^2 g_1^2}{16 g_0^2} + \frac{\kappa^2 g_1}{2g_0}\cos(2\kappa x) + \\ + \frac{3\kappa^2 g_1^2}{16 g_0^2}\cos(4\kappa x) + \left[\frac{\kappa g_1}{2g_0}\sin(2\kappa x)\right]\frac{\partial}{\partial x}. \quad (8)$$

We take the wave function in the form

$$\phi(x,t) = R(x)\exp\{i[\theta(x) - \mu t]\}$$

with $\theta(x)$ and $\mu$ being respectively the phase and the chemical potential. Substituting in Eq. (6) produces a hydrodynamic version of the nonlinear Schrödinger (NLS) equation expressed as

$$\frac{d^2R}{dx^2} + 2\tilde{\mu}R - 2R^3 - R\left(\frac{d\theta}{dx}\right)^2 - 2V_1\sin(2Kx)R - \\ - \left[\kappa\varepsilon\cos(2\kappa x) + \frac{3}{8}\varepsilon^2\cos(4\kappa x)\right]R - \\ - \varepsilon\sin(2\kappa x)\frac{dR}{dx} = 0, \quad (9)$$

$$\frac{d}{dx}\left(R^2\frac{d\theta}{dx}\right) = \varepsilon\sin(2\kappa x)R^2\frac{d\theta}{dx}. \quad (10)$$

In Eqs. (9) and (10), we have set

$$2\tilde{\mu} = 2\mu + 3\varepsilon^2/8$$

and the parameter

$$\varepsilon = \kappa g_1/g_0 \ll 1$$

is small due to the inequality $g_0 \gg g_1$. The first derivative $d\theta/dx$ in Eq. (10) represents the velocity and $R^2 = n$ is the number density of atoms of the system described by Eq. (6) [46]. Thereby, Eq. (10) suggests the existence of the spatially varying atomic current

$$J = R^2\frac{d\theta}{dx} = \Gamma\exp\left[-\frac{\varepsilon\cos(2\kappa x)}{2\kappa}\right] \quad (11)$$

in the system described by Eq. (6). Here, $\Gamma$ is an integral constant determined by the initial and boundary conditions. We note that the true number density of atoms is not $R^2$ but $|\psi|^2$ [46]. Accordingly, $J$ is not the true atomic current of the BEC. But, obviously, $R^2$ and $J$ are respectively proportional to the true number density of atoms and atomic current. As in Ref. [46], we treat $R^2$ and $J$ as the number density of atoms and the atomic current of system (6). Given the above discussion and after careful inspection, we can find that Eqs. (9) and (11) are similar to the equations of motion of a classical Newtonian particle in a central field; the coordinate $x$ plays the role of time $t$, and $J$ is proportional to the angular momentum.

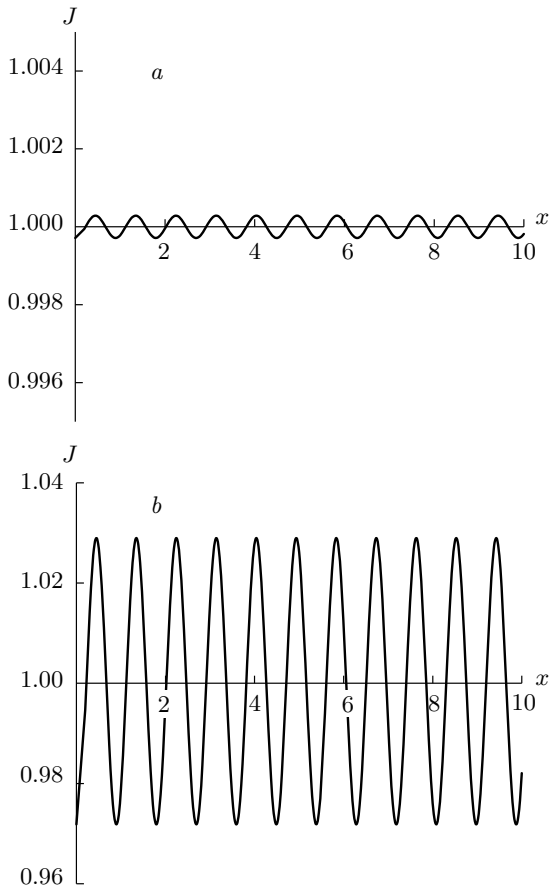


**Fig. 1.** Spatial evolutions of the current with $\kappa = 3.5$, $\Gamma = 1$, $\varepsilon = 0.002$ ($a$) and $0.2$ ($b$)

In Refs. [18–21], the nonlinearity parameters are fixed and the atomic currents are steady flows. But when the nonlinearity parameter is spatially dependent, the atomic current is spatially modulated, as can be judged from Eq. (11).

Equation (11) implies that there exists a spatially dependent atomic current in the condensate. The inclusion of $\kappa$ and $\varepsilon$ related to the spatially dependent nonlinear parameter in Eq. (11) means that the atomic current can be adjusted via the Feshbach resonance.

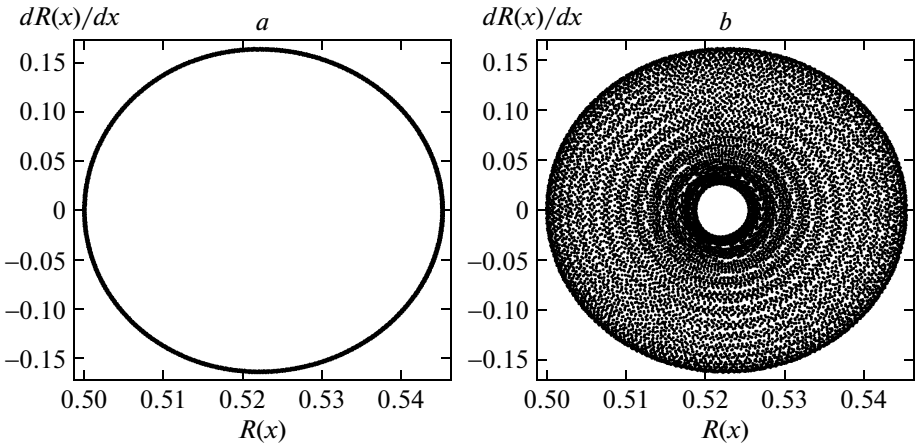


**Fig. 2.** Phase portraits in the plane $(R(x), \dot{R}(x))$ for $\varepsilon = 0.002$ $(a)$ and $\varepsilon = 0.2$ $(b)$, with $\tilde{\mu} = 7$, $V_1 = 0.001$, $\kappa = 3.5$, $\Gamma = 1$, $K = 4.5$, $R(0) = 0.5$, and $\dot{R}(0) = 0$

Undoubtedly, the current exerts an important effect on the spatial distribution of BEC atoms due to the transportation of BEC atoms within the system itself. In Fig. 1, we numerically demonstrate the spatially dependent current with $\kappa = 3.5$, $\Gamma = 1$, and different values of $\varepsilon$. We see from Fig. 1$a$ that the oscillating amplitude of the current is small when $\varepsilon = 0.002$. Keeping the values of $\kappa$ and $\Gamma$ fixed and increasing $\varepsilon$ to 0.2 leads to a much larger oscillating amplitude of the current in Fig. 1$b$. According to Eq. (11) and Fig. 1, we can conclude that irrespective of the values of the other parameters, the current always oscillates around the value $\Gamma$, namely the average intensity of the current is $\Gamma$. It has been pointed out that $\Gamma$ is determined by the initial and boundary conditions. This means that the initial and boundary conditions can exert very strong influence on the intensity of the current. To summarize, the oscillating amplitude of the current can be adjusted by the Feshbach resonance and the intensity of the current depends heavily on the initial and boundary conditions.

To intuitively observe the effect of the atomic current on the spatial distribution of condensed atoms, we numerically solve Eq. (9) in a space interval from $x = 0$ to $x = 500$ and plot the phase portraits in the plane $(R(x), \dot{R}(x))$ (see Fig. 2). We have set the parameters and initial conditions as $\tilde{\mu} = 7$, $V_1 = 0.001$, $\kappa = 3.5$, $\Gamma = 1$, $K = 4.5$, $R(0) = 0.5$, $\dot{R}(0) = 0$, $\varepsilon = 0.002$ in Fig. 2$a$, and $\varepsilon = 0.2$ in Fig. 2$b$. When $\varepsilon = 0.002$, we observe from Fig. 2$a$ that there is only one closed orbit in the phase space, indicating that the system is in a single-periodic state. But as $\varepsilon$ increases to 0.2, the system is in a very complex or even chaotic state, as shown in Fig. 2$b$. By contrasting Figs. 2$a$ and $b$, we can conclude that a strong enough oscillation of the current can take the system to a very complex or even chaotic state. In reality, a strong oscillation of the current means a strong modulation of the nonlinear interaction between atoms, which must result in a complex spatial distribution or even completely chaotic spatial distribution of condensed atoms.

## 3. THE CASE WITH A CONSTANT PHASE

The complexity of Eq. (9) indicates that it is difficult to find its exact solution by analytic methods. But when the phase is constant, for example, in the case of a standing wave with $\theta = 0$, the atomic current disappears and we arrive at

$$\frac{d^2R}{dx^2} + 2\tilde{\mu}R - 2R^3 - 2V_1 \sin(2Kx)R - \\ - \left[\kappa\varepsilon\cos(2\kappa x) + \frac{3}{8}\varepsilon^2\cos(4\kappa x)\right]R - \\ - \varepsilon\sin(2\kappa x)\frac{dR}{dx} = 0. \quad (12)$$

If the coordinate $x$ is replaced with time $t$, Eq. (12) is just a driven Duffing equation with damping. To perform a perturbative analysis, we assume that

$$V_1 = \varepsilon v_1$$

and change Eq. (12) into the perturbed form

$$\frac{d^2R}{dx^2} + 2\tilde{\mu}R - 2R^3 = 2\varepsilon v_1 \sin(2Kx)R + \left[\kappa\varepsilon\cos(2\kappa x) + \frac{3}{8}\varepsilon^2\cos(4\kappa x)\right]R + \varepsilon\sin(2\kappa x)\frac{dR}{dx}. \quad (13)$$

Expanding a solution of Eq. (13) to the first order

$$R = R_0 + \varepsilon R_1, \quad (14)$$

and substituting it in Eq. (13), we obtain the zeroth-order unperturbed equation

$$\frac{d^2R_0}{dx^2} + 2\tilde{\mu}R_0 - 2R_0^3 = 0 \quad (15)$$

and the first-order equation

$$\frac{d^2R_1}{dx^2} + 2\tilde{\mu}R_1 - 6R_0^2R_1 = \gamma_1 \quad (16)$$

with

$$\gamma_1 = \frac{dR_0}{dx}\sin(2\kappa x) + [\kappa\cos(2\kappa x) + 2v_1\sin(2Kx)]R_0.$$

Zeroth-order equation (15) is just the Duffing equation, admitting the famous heteroclinic solution

$$R_0 = \sqrt{\tilde{\mu}}\,\mathrm{th}\left[\sqrt{\tilde{\mu}}(x-C)\right], \quad (17)$$

where

$$C = x_0 - \mathrm{th}^{-1}\left[R_0(x_0)/\sqrt{\tilde{\mu}}\right]/\sqrt{\tilde{\mu}}$$

is a constant determined by the initial and boundary conditions for $\tilde{\mu} > 0$. In the phase space of unperturbed system (15), the separatrix is just formed by the heteroclinic orbits corresponding to the heteroclinic solutions. In our theoretic analysis, what we are interested in whether the system phase space structure is close to the separatrix. If the unperturbed system is subject to various forces, complicated and even chaotic space structures may appear in the vicinity of the separatrix.

According to [16], when $\gamma_1 = 0$, using heteroclinic solution (17), we can easily obtain two linearly independent solutions of Eq. (16) as

$$f_1 = \frac{dR_0}{dx} = \tilde{\mu}\,\mathrm{sech}^2\left[\sqrt{\tilde{\mu}}(x-C)\right], \quad (18)$$

$$f_2 = \frac{dR_0}{dx}\int\left(\frac{dR_0}{dx}\right)^{-2}dx = \frac{3}{8\tilde{\mu}}(x-C)\,\mathrm{sech}^2\left[\sqrt{\tilde{\mu}}(x-C)\right] + \frac{1}{8\tilde{\mu}^{3/2}}\left\{\mathrm{sh}\left[2\sqrt{\tilde{\mu}}(x-C)\right] + 3\,\mathrm{th}\left[\sqrt{\tilde{\mu}}(x-C)\right]\right\}. \quad (19)$$

It is obvious that $f_2$ is unbounded and exponentially increases as $x$ increases because it involves the hyperbolic sine function. Using the two linearly independent solutions, we can construct the general solution of Eq. (16) as [17]

$$R_1(x) = f_2\int_{C_1}^{x} f_1\gamma_1 dx - f_1\int_{C_2}^{x} f_2\gamma_1 dx, \quad (20)$$

where $C_1$ and $C_2$ are two arbitrary constants determined by initial conditions. This solution can be directly proved by comparing the second derivative $R_{1xx}$ from Eq. (20) with that in Eq. (16). It is not difficult to verify that the general solution (20) is usually unbounded due to the exponentially increasing function $f_2$. In other words, the density of the condensed atoms be very large, similarly to the case where the density is very large at the origin of the vertical coordinate [2]. But if the condition

$$I_{\pm} = \lim_{x\to\pm\infty}\int_{C_1}^{x} f_1\gamma_1 dx = 0 \quad (21)$$

is satisfied, then this kind of unboundedness can be effectively avoided. Inspecting Eq. (21) carefully, we find that

$$I_+ - I_- = 0$$

can eliminate the constant $C_1$ and produce the famous Melnikov function

$$M(x_0) = I_+ - I_- = \int_{-\infty}^{\infty} f_1\gamma_1 dx = 0. \quad (22)$$

Performing the integration in Eq. (22), we obtain

$$M(x_0) = 2\pi\kappa\left[\frac{2}{3}(\kappa^2+\tilde{\mu}) - \kappa^2\right]\mathrm{csch}\left(\frac{\pi\kappa}{\sqrt{\tilde{\mu}}}\right)\times \sin(2\kappa C) + 4\pi v_1K^2\mathrm{csch}\left(\frac{\pi K}{\sqrt{\tilde{\mu}}}\right)\times \cos(2KC) = 0. \quad (23)$$

As is well known, the Melnikov function is also called the Melnikov distance between the stable and unstable manifolds in the Poincaré section at $x_0$. If the Melnikov function $M(x_0)$ has simple zeros, there exists Smale-horseshoe chaos in the system. Thereby a simple zero Melnikov function $M(x_0)$ can lead to a chaotic spatial structure of the condensate.

Equations (22) and (23) indicate that boundedness condition (21) contains the Melnikov chaotic criterion predicting the onset of chaotic spatial structure. In

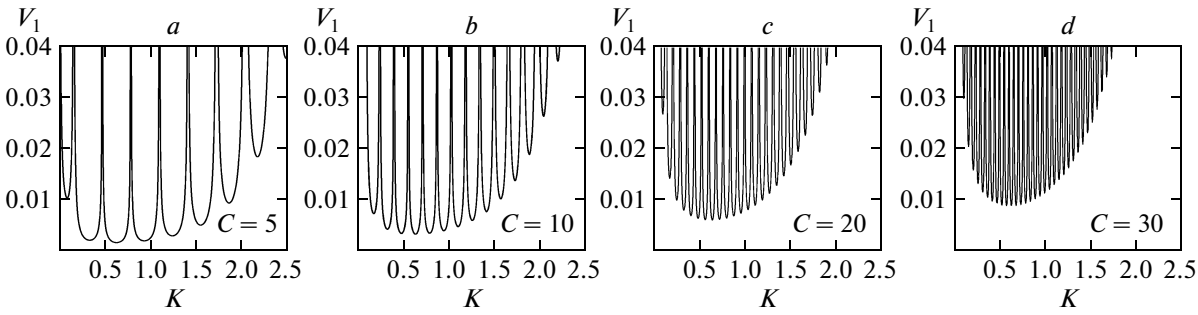


**Fig. 3.** Stability curves for different initial conditions; $\tilde{\mu} = 1.0$, $\kappa = 2.5$

other words, if Eq. (21) is satisfied, then Eqs. (22) and (23) are satisfied automatically. Consequently, the general solution of Eqs. (22) and (23) must be bounded and chaotic. In fact, carefully inspecting the general solution (20), we can see that its first term is the unbounded function $f_2$ times an analytically unsolvable integration. The product can be bounded if and only if boundedness conditions (21) and (22) are strictly satisfied, which manifests that the chaotic spatial structure of the system is extremely sensitive to the initial conditions and system parameters. Any infinitesimal deviations from the conditions and system parameters under Eqs. (21) and (22) are exponentially amplified due to the exponential increase of $f_2$ as $x \to \pm\infty$. Unfortunately, such deviations cannot be avoided in calculations anyhow, irrespective of the adopted numerical integration methods and steps and number precisions. The unsolvable integration in Eq. (20) cannot be expressed in finite form in elementary functions, and Eq. (23) shows the relevance of parameters to the irrational number $\pi$ with an infinite sequence of digits, which would cause inaccuracy in determining the values of parameters. In short, given the foregoing analysis, the spatial structure of the condensate is unpredictable. That is a significant property of chaos.

Melnikov function (23) contains the parameter $C$ determined by the initial conditions, showing that the stability of the system satisfying $M(x_0) = 0$ is sensitively dependent on the initial conditions. This is one of the leading features of strange chaotic attractors. To clearly see the dependence on the initial conditions, in Fig. 3 we plot the stability curves in the $(K,\ V_1)$ plane from Eq. (23) for different values of $C$ with $\tilde{\mu} = 1.0$ and $\kappa = 2.5$. We see from Fig. 3, that as the value of $C$ increases, the stability curves become greater in number and denser. This signifies the existence of a chaotic spatial structure in the condensate [16].

In Fig. 4, we display the parameter regions in the

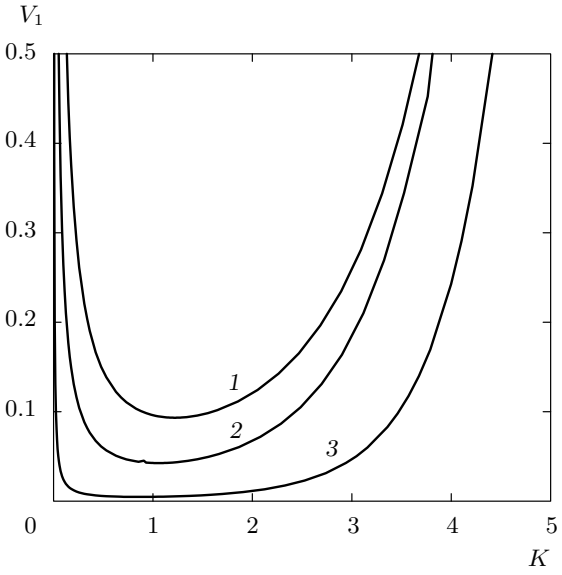


**Fig. 4.** The regions of regular and chaotic states for different values of $\tilde{\mu} = 4$ (*1*), 3 (*2*), 2 (*3*). The regions above the curves correspond to chaotic states and the regions below correspond to regular states; $\kappa = 1.9$, $C = 10$

$(K,\ V_1)$ plane for different values of $\tilde{\mu}$ with $\kappa = 1.9$ and $C = 10$ based on Eq. (23). The regions above the curves correspond to the chaotic states and those below correspond to the regular states. The values of $v_1$ on the curves are those of the thresholds. We can see from Fig. 4 that as the dimensionless chemical potential $\tilde{\mu}$ increases, the chaotic region is reduced. This means that a large chemical potential can lead to chaos suppression.

To verify the validity of the above analyses, after carefully selecting parameters above the critical curve (corresponding to $\tilde{\mu} = 2$) in Fig. 4, we numerically solve Eq. (12) in the space interval from $x = 0$ to $x = 500$

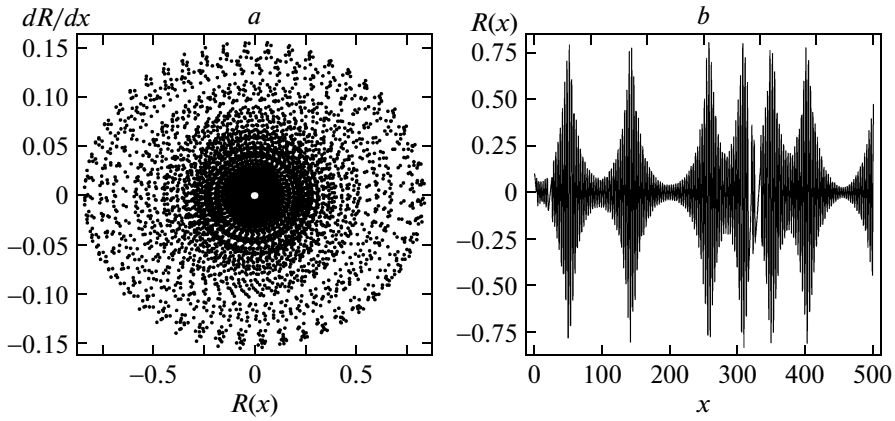


**Fig. 5.** ($a$) Phase portrait in the plane $(R(x), \dot{R}(x))$; ($b$) spatial evolution of $R(x)$. Both the phase portrait and the spatial evolution show that the system is in a chaotic state; $\tilde{\mu} = 2.0$, $V_1 = 0.3$, $\varepsilon = 0.15$, $\kappa = 1.9$, $K = 1.95$, $R(0) = 0.1$, and $\dot{R}(0) = 0$

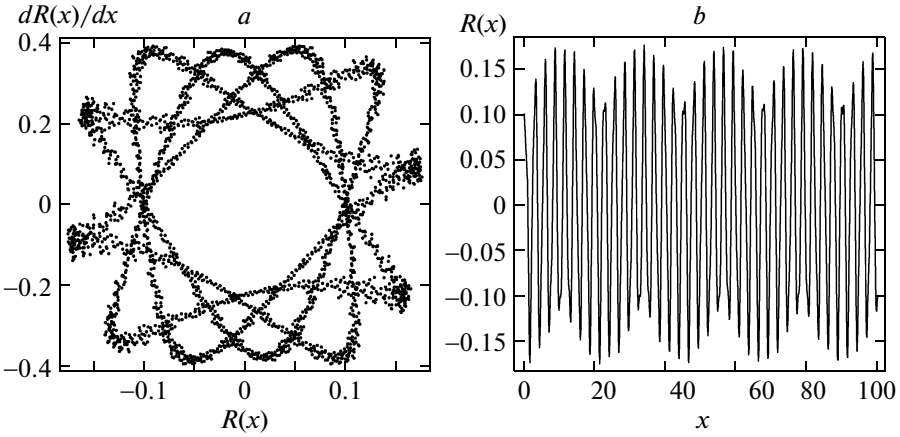


**Fig. 6.** ($a$) Phase portrait in the plane $(R(x), \dot{R}(x))$; ($b$) spatial evolution of $R(x)$. Both the phase portrait and the spatial evolution show that the system is in a quasiperiodic state; $\tilde{\mu} = 2.0$, $V_1 = 4$, $\varepsilon = 0.2$, $\kappa = 3$, $K = 3.5$, $R(0) = 0.1$, and $\dot{R}(0) = 0$

and plot the results in Fig. 5 for $\tilde{\mu} = 2.0$, $V_1 = 0.3$, $\varepsilon = 0.15$, $\kappa = 1.9$, $K = 1.95$, $R(0) = 0.1$, and $\dot{R}(0) = 0$. From the phase portrait in Fig. 5$a$, we can see a typically chaotic attractor, which implies that the system is in a chaotic state; this fact is also proved by the corresponding chaotic spatial evolution of $R(x)$ shown in Fig. 5$b$. The numerical simulations are shown to agree with our analytic results.

As the value of $V_1$ increases gradually, the above analytic methods become inaccurate, and even invalid. In such cases, we can resort to numerical simulations.

After setting $\tilde{\mu} = 2.0$, $\varepsilon = 0.2$, $\kappa = 3$, $K = 3.5$, $R(0) = 0.1$, and $\dot{R}(0) = 0$, we numerically solve Eq. (12) with different values of $V_1$ and plot phase portraits in the plane $(R(x), \dot{R}(x))$ and the corresponding spatial evolutions of $R(x)$ in Figs. 6 and 7 from $x = 0$ to $x = 500$. When $V_1 = 4$, from the phase portrait in Fig. 6$a$ we can see typical quasiperiodic orbits indicating that system is in a quasiperiodic state; the corresponding spatial evolution of $R(x)$ also indicates that the system is in a quasiperiodic state (see Fig. 6$b$). Both the phase portrait and spatial evolution of $R(x)$ in Fig. 6 show that BEC atoms are in a quasiperiodic spatial distribution. But as $V_1$ increases to 8.2 and the other parameters and initial conditions are fixed, a typically chaotic phase portrait appears, as can be seen in Fig. 7$a$; Fig. 7$b$ is the corresponding chaotic spatial evolution of $R(x)$. This signifies that BEC atoms are in a chaotic spatial distribution. For visual clarity, we only plot the spatial evolutions of $R(x)$ from $x = 0$

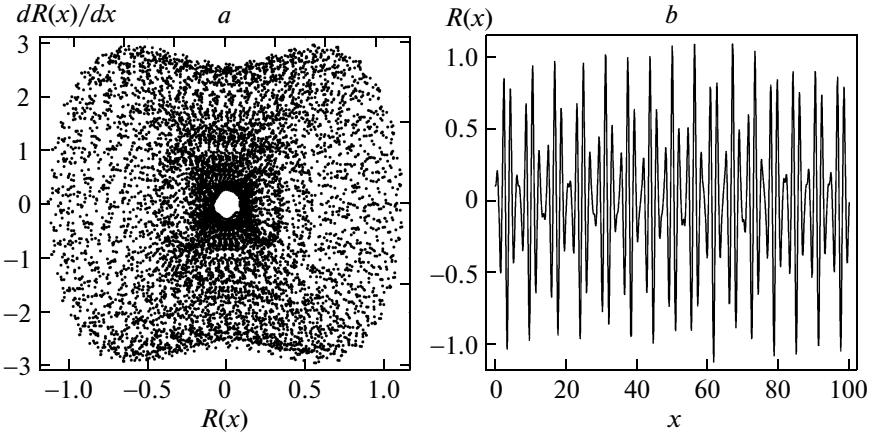


**Fig. 7.** ($a$) Phase portrait in the plane $(R(x), \dot{R}(x))$; ($b$) spatial evolution of $R(x)$. Both the phase portrait and the spatial evolution show that the system is in a chaotic state. Here, $V_1 = 8.2$ and the other parameters and initial conditions are the same as in Fig. 6

to $x = 100$. Figures 6 and 7 illustrate that for a set of specific parameters and initial conditions, increasing the value of $V_1$ can lead BEC atoms to a chaotic spatial distribution via a quasiperiodic route.

## 4. CONCLUSION

In this work, we have investigated the spatial structure of a collisionally inhomogeneous BEC. When the BEC phase is spatially dependent, a spatially varying atomic current with an explicit analytic expression appears in the system. Theoretical analyses reveal that the oscillating amplitude of the current can be adjusted via the Feshbach resonance. A strong oscillation of the current can lead the system to a very complex spatial distribution of BEC atoms.

For the case with a constant BEC phase, the abovementioned current disappears and the equation of the system takes the form of a driven Duffing equation with damping. By a perturbative analyses, we obtain the Melnikov chaotic criterion predicting the existence of a chaotic spatial distribution of condensed atoms. Numerical simulations show that the system can step from a quasiperiodic state into a chaotic one with an increasing depth of the external optical lattice.

Chaos in a BEC system may have negative effect on the stability and manipulation of the system itself. It was shown in Ref. [14] that chaos in BECs is connected with its collapsing process. Therefore, studies of chaos in BECs are very helpful in maintaining the stability of BECs. On the other hand, a BEC system is an important candidate for quantum computation [51]. However, chaos is usually associated with quantum entanglement, exerting great effect on quantum computation [52, 53]. Undoubtedly, studies on chaos in BECs are of theoretical and experimental necessity.

This work is supported by the National Natural Science Foundation of China (11204076, 11147011), the Scientific Research Fund of Hunan Provincial Education Department (08c344), and the Opening Project of Key Laboratory of Low-Dimensional Quantum Structures and Quantum Control (Hunan Normal University), Ministry of Education (QSQC1005)).

## REFERENCES

1. M. BenDahan, E. Peik, J. Reichel, Y. Castin, and C. Salomon, Phys. Rev. Lett. **76**, 4508 (1996).

2. B. P. Anderson and M. A. Kasevich, Science **282**, 1686 (1998).

3. N. K. Efremidis, S. Sears, D. N. Christodoulides, J. W. Fleischer, and M. Segev, Phys. Rev. E **66**, 046602 (2002).

4. M. Greiner, O. Mandel, T. Esslinger, T. W. Hänsch, and I. Bloch, Nature (London) **415**, 39 (2002); D. Oosten, P. Straten, and H. Stoof, Phys. Rev. A **63**, 053601 (2001).

5. O. Morsch, J. H. Müller, M. Cristiani, D. Ciampini, and E. Arimondo, Phys. Rev. Lett. **87**, 140402 (2001).

6. Z. W. Xie, W. P. Zhang, S. T. Chui, and W. M. Liu, Phys. Rev. A **69**, 053609 (2004).

**7**. S. Burger, F. S. Cataliotti, C. Fort, F. Minardi, M. Inguscio, M. L. Chiofalo, and M. P. Tosi, Phys. Rev. Lett. **86**, 4447 (2001).

**8**. F. S. Cataliotti, S. Burger, C. Fort, P. Maddaloni, F. Minardi, A. Trombettoni, A. Smerzi, and M. Inguscio, Science **293**, 843 (2001).

**9**. B. Wu and Q. Niu, Phys. Rev. A **64**, 061603(R) (2001).

**10**. M. Cristiani, O. Morsch, J. H. Müller, D. Ciampini, and E. Arimondo, Phys. Rev. A **65**, 063612 (2002).

**11**. J. Liu, L. Fu, B. Ou, S. Chen, D. Choi, B. Wu, and Q. Niu, Phys. Rev. A **66**, 023404 (2002).

**12**. D. Choi and B. Wu, Phys. Lett. A **318**, 558 (2003).

**13**. C. Orzel, A. K. Tuchman, M. L. Fenselau, M. Yasuda, and M. A. Kasevich, Science **291**, 2386 (2001).

**14**. V. S. Filho, A. Gammal, T. Frederico, and Lauro Tomio, Phys. Rev. A **62**, 033605 (2000).

**15**. P. Muruganandam and S. K. Adhikari, Phys. Rev. A **65**, 043608 (2002).

**16**. C. Lee, W. Hai, L. Shi, X. Zhu, and K. Gao, Phys. Rev. A **64**, 053604 (2001).

**17**. W. Hai, C. Lee, G. Chong, and L. Shi, Phys. Rev. E **66**, 026202 (2002).

**18**. W. Hai, S. Rong, and Q. Zhu, Phys. Rev. E **78**, 066214 (2008).

**19**. G. Chong, W. Hai, and Q. Xie, Chaos **14**, 217 (2004).

**20**. J. Fang and W. Hai, Physica B **370**, 61 (2005).

**21**. F. Li, Z. Ren, H. Luo, W. Shu, and Q. Wu, Commun. Theor. Phys. **48**, 107 (2007); F. Li, D. Zhang, and W. Li, Acta Phys. Sin. **60**, 120304 (2011).

**22**. W. Hai, G. Lu, and H. Zhong, Phys. Rev. A **79**, 053610 (2009).

**23**. W. Hai, Q. Zhu, and S. Rong, Phys. Rev. A **79**, 023603 (2009).

**24**. Q. Xie, W. Hai, and G. Chong, Chaos **13**, 801 (2003).

**25**. F. Li, W. Shu, H. Luo, and Z. Ren, Chin. Phys. **16**, 650 (2007).

**26**. J. Fang, W. Hai, G. Chong, and Q. Xie, Physica A **349**, 133 (2005).

**27**. B. Gertjerenken, S. Arlinghaus, N. Teichmann, and C. Weiss, Phys. Rev. A **82**, 023620 (2010).

**28**. I. Březinová, A. Lode, A. Streltsov, O. Alon, L. Cederbaum, and J. Burgdörfer, Phys. Rev. A **86**, 013630 (2012).

**29**. F. Li, W. Shu, J. Jiang, H. Luo, and Z. Ren, Europ. Phys. J. D **41**, 355 (2007).

**30**. G. Chong, W. Hai, and Q. Xie, Phys. Rev. E **70**, 036213 (2004); *ibid.* **71**, 016202 (2005).

**31**. M. Edwards, L. M. DeBeer, M. Demenikov, J. Galbreath, T. Mahaney, B. Nelsen, and C. Clark, J. Phys. B **38**, 363 (2005).

**32**. J. Denschlag, J. Simsarian, H. Häffner, C. McKenzie, A. Browaeys, D. Cho, K. Helmerson, S. Rolston, and W. Phillips, J. Phys. B **35**, 3095 (2002).

**33**. P. A. Ruprecht, M. Edwards, K. Burnett, and C. W. Clark, Phys. Rev. A **54**, 4187 (1996).

**34**. Y. B. Band and M. Sokuler, Phys. Rev. A **66**, 043614 (2002).

**35**. L. Fallani, F. S. Cataliotti, J. Catani, C. Fort, M. Modugno, M. Zawada, and M. Inguscio, Phys. Rev. Lett. **91**, 240405 (2003).

**36**. P. Öhberg and S. Stenholm, J. Phys. B **32**, 1959 (1999).

**37**. A. S. Mellish, G. Duffy, C. McKenzie, R. Geursen, and A. C. Wilson, Phys. Rev. A **68**, 051601(R) (2003).

**38**. P. Kevrekidis, D. Frantzeskakis, R. Carretero-González, B. Malomed, G. Herring, and A. Bishop, Phys. Rev. A **71**, 023614 (2005).

**39**. L. Fallani, L. De Sarlo, J. Lye, M. Modugno, R. Saers, C. Fort, and M. Inguscio, Phys. Rev. Lett. **93**, 140406 (2004).

**40**. F. Kh. Abdullaev, J. G. Caputo, R. A. Kraenkel, and B. A. Malomed, Phys. Rev. A **67**, 013605 (2003); H. Saito and M. Ueda, Phys. Rev. Lett. **90**, 040403 (2003).

**41**. A. J. Moerdijk, B. J. Verhaar, and A. Axelsson, Phys. Rev. A **51**, 4852 (1995).

**42**. J. L. Roberts, N. R. Claussen, J. P. Burke, C. H. Greene, E. A. Cornell, and C. E. Wieman, Phys. Rev. Lett. **81**, 5109 (1998).

**43**. J. Stenger, S. Inouye, M. R. Andrews, H. J. Miesner, D. M. Stamper-Kurn, and W. Ketterle, Phys. Rev. Lett. **82**, 2422 (1999).

**44**. P. G. Kevrekidis, G. Theocharis, D. J. Frantzeskakis, and B. A. Malomed, Phys. Rev. Lett. **90**, 230401 (2003).

**45**. M. A. Porter, P. G. Kevrekidis, B. A. Malomed, and D. J. Frantzeskakis, Physica D **229**, 104 (2007).

**46**. G. Theocharis, P. Schmelcher, P. G. Kevrekidis, and D. J. Frantzeskakis, Phys. Rev. A **72**, 033614 (2005); *ibid.* **74**, 053614 (2006).

**47**. F. Kh. Abdullaev and J. Garnier, Phys. Rev. A **72**, 061605(R) (2005).

**48**. H. Sakaguchi and B. A. Malomed, Phys. Rev. E **72**, 046610 (2005).

**49**. P. Niarchou, G. Theocharis, P. Kevrekidis, P. Schmelcher, and D. Frantzeskakis, Phys. Rev. A **76**, 023615 (2007).

**50**. A. Rodrigues, P. Kevrekidis, M. Porter, D. Frantzeskakis, P. Schmelcher, and A. R. Bishop, Phys. Rev. A **78**, 013611 (2008).

**51**. S. Sklarz, I. Friedler, D. Tannor, Y. Band, and C. Williams, Phys. Rev. A **66**, 053620 (2002).

**52**. K. Furuya, M. C. Nemes, and G. Q. Pellegrino, Phys. Rev. Lett. **80**, 5524 (1998).

**53**. J. N. Bandyopadhyay and A. Lakshminarayan, Phys. Rev. Lett. **89**, 060402 (2002).